S1 Control run

Here, we present results from the control run (CTR). To get an overview over the model's performance, we compare them to observations of sea ice (Cavalieri et al., 1996) and ocean temperature and salinity (Orsi and Whitworth, 2005). For the sea ice characteristics, the main focus is on the last decade (2004-2013), since it will be used for the comparison in Section 3. For the water characteristics, the model data from the year corresponding to the observation was used.

S1.1 Sea ice characteristics

The modeled sea ice concentration around Antarctica is compared with data obtained from passive microwave data sensors (Cavalieri et al., 1996) in Figure S1a-d. The model result matches the observations very well. It successfully reproduces the spatial distribution for both the minimum sea ice extent in March and the maximum sea ice extent in September. In March, a sea ice maximum is found in the western Weddell Sea. Also the Ross and Amundsen Seas feature large remnants of the ice cover, while less sea ice is found along the coastline of East Antarctica. However, the March ice concentration in the simulation tends to be lower than in the satellite data.

In September, the model features a sea ice outline that matches the observed shape very well. We find northward outcrops of the sea ice east of the South Sandwich Islands (approx. 27° W), west of the southward bend of the Southwest Indian Ridge (approx. 15° E), close to the Kerguelen Plateau (approx. 80° E), at the eastern margin of the d'Urville Sea (approx. 155° E), and east of the Pacific Antarctic Ridge (approx. 152° W). While the observed sea ice covered area is matched very well by the model, the sea ice concentrations in September are slightly overestimated.

The confines of the sea ice covered area in winter are defined by the Antarctic circumpolar current (ACC). The warm surface temperatures of the ACC melt the ice and thus inhibit sea ice expansion. The larger discrepancies between model and observation can therefore be mainly attributed to the resolution of the bathymetry, which steers the ocean currents.

A time series of the sea ice extent for both, simulation and observation is calculated from the sea ice concentration data using a threshold of 15%. The mean seasonal cycle of the sea ice extent (Figure S1e) shows that CTR very well captures amplitude and range of the seasonal changes. The extremes in summer and winter are very close to the observations and also during the freezing period, the simulated sea ice extent does not differ far from the observations. Only during the melting season, the simulation features a considerably higher sea ice extent than observed. This indicates a delay in the onset of sea ice melting that can be explained by the overestimation of ice concentrations in winter. It is compensated by much faster melting toward the end of summer, which is due to a shallower summer mixed layer of the model leading to an overestimation of ocean surface temperatures.

A time series of the deviations of the sea ice extent from the mean seasonal cycle (Figure S1f) features periods of large discrepancies during the first decade. Thereafter, the differences between CTR and observations in the sea ice extent are smaller and the short-term anomalies of the sea ice extent show similar fluctuations in CTR and in the satellite observations.

The initially high but later diminished discrepancies between simulation and observation indicate that after 10 years the model is close to equilibrium. In the period 1989-2013, the short-term fluctuations of the sea ice extent predominantly seem to be caused by similar events in model and observation. Although resolution remains an ever-present challenge in sea ice modeling, the 0.25° resolution of the model proves high enough to transmit the most important fluctuations of atmosphere and ocean to the sea ice.

The trend for the sea ice extent calculated for the period 1989-2013 from the simulation (31.000 km^2 yr^{-1}) matches the corresponding trend from the observations (25.000 km^2 yr^{-1}) fairly well. However, the simulation's trend decreases for later (shorter) periods and turns even slightly negative for the last decade. Since this behavior is not seen in the observations, the model is evidently missing an aspect of the development of the sea ice extent and the atmosphere (in the simulation) can not by itself account for the change. It is therefore a likely assumption that changes (increase) in the Antarctic runoff, a probable driving force behind the positive trend, are the missing piece in the puzzle.

For other sea ice characteristics there is still only sparse data available and a comprehensive comparison between model results and observations is not yet possible. However, the sea ice thickness of CTR (Figure S2a) is close to expectations. Typically the highest sea ice thicknesses are found close to the continent, while the areas farther offshore are covered with thinner ice. In the Weddell and Ross Seas, we can see the northward transport of the sea ice leaving traces in the thickness distribution. The coastal westward drift (Figure S2b) leads to dynamic build up of the sea ice thickness on the eastern flanks of the coastline while the western flanks are typically accompanied by a minimum in ice thickness.

The long-term mean sea ice velocities are strongly influenced by the ocean surface velocities. In the ocean, the westward coastal current following the continental shelf break is connected to the eastward ACC by the cyclonic subpolar gyres. In the Ross Sea, we find the Ross Gyre not only exporting sea ice northward on its western branch, but also causing southward drift of sea ice on its eastern branch, although to a much smaller extent. The Weddell Gyre has a less well-defined eastern, southward branch, due to its greater variability, and there is no southward ice drift visible in the long-term mean.

S1.2 Water characteristics

In this chapter, salinity and potential temperature of CTR are compared to observations on two vertical sections through the Weddell and the Ross Seas. The measurements were taken during 1995 and 1992, respectively, and are compared to the annual mean of the corresponding year from the simulation.

The salinity and temperature section of CTR in the Weddell Sea from 15° W, 75° S to 37° W, 30° S is compared to the World Ocean Circulation Experiment (WOCE) Southern Ocean Atlas (Orsi and Whitworth, 2005) section A23 (Figure S3). The comparison shows, that the model performs very well in reproducing the general characteristics of the different water masses. In the south close to the Antarctic continent, we find very cold and fresh waters at the surface with minimum temperatures close to the freezing point. Below the surface layer, we find slightly warmer and more saline waters, the Warm Deep Water (WDW), with a maximum in temperatures and salinity at ca. 400 m depth. With salinities slightly over 34.7 and temperatures reaching 1.4° C the simulation overestimates the maximum of the WDW. Below the WDW, salinity and temperature decrease again toward the bottom, where salinities below 34.66 and temperatures below -0.7° C are reached in the simulation. Compared to the observation the model's bottom values are slightly too high.

In the north, the surface waters are several degrees warmer than in the south and temperatures decrease with depth, reaching -0.4° C at the bottom. Salinities, however, increase with depth in the upper ocean and we find a maximum of over 34.76 at depths of 1500-2000 m, below which salinities slightly decrease again to less than 34.66 at the bottom.

The slight overestimation of salinity and temperature of the WDW in the Weddell Gyre can be attributed to the fact that the coarser model topography allows the waters of the ACC to mix more easily with those of the gyre over the South Scotia Ridge.

Also the bottom water in the Weddell Basin is slightly too warm and too saline. Apart from deficiencies in the topography of the South Scotia Ridge, that might let the dense water escape more easily into the open ocean, it is a common problem for OGCMs to correctly reproduce the modification of dense shelf water and ensuing formation of bottom water. While sinking down along the continental slope, the dense waters lose their characteristics too fast due to the model's limitations in resolution.

Another section of salinity and potential temperature in the eastern Ross Sea at 150° W also shows very good agreement between model and observation (WOCE section P16) (Figure S4). At the surface, we find cold and fresh ($S \approx 34.0$) waters close to the Antarctic continent and warm, slightly saltier ($S \approx 34.5$) waters in the north. At the bottom, we see the saline ($S > 34.7$) and relatively cold ($T < 0.8$° C) waters from Antarctica spill over the topographic obstacle of the Pacific Antarctic Ridge into the world ocean. In the simulation, the bottom waters retained in the southern basin close to the Antarctic continent with temperatures of approx. 0.9° C and salinities of approx. 34.7 are slightly warmer and more saline than in the observation. As in the Weddell Sea, two processes can contribute to this: First, the coarseness of the bathymetry in the model allows the dense water to escape more easily from the basin, and second, the resolution of the model hinders the production of the dense deep waters.

References

Cavalieri, D. J., Parkinson, C. L., Gloersen, P., and Zwally, H.: Sea Ice Concentrations from Nimbus-7 SMMR and DMSP SSM/I-SSMIS Passive Microwave Data. Boulder, Colorado USA: NASA National Snow and Ice Data Center Distributed Active Archive Center, 1996, updated yearly.

Orsi, A. H. and Whitworth III, T.: Hydrographic Atlas of the World Ocean Circulation Experiment (WOCE), Volume 1: Southern Ocean. (eds. Sparrow, M., Chapman, P. and Gould, J.), International WOCE Project Office, Southampton, U.K., http://woceatlas.tamu.edu, 2005.

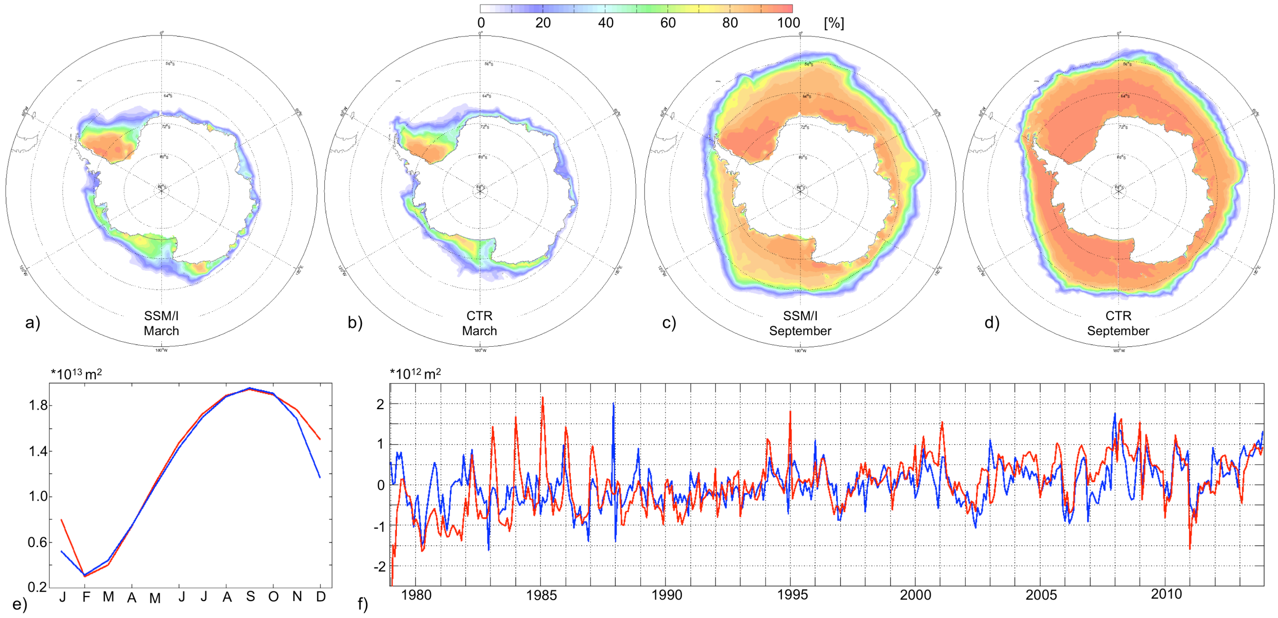

Figure S1: a-d) Sea ice concentrations, mean 2004-2013; e) mean seasonal cycle of sea ice extent 1979-2013 and f) divergence from mean seasonal cycle of sea ice extent, SSM/I observations (blue) and CTR (red).

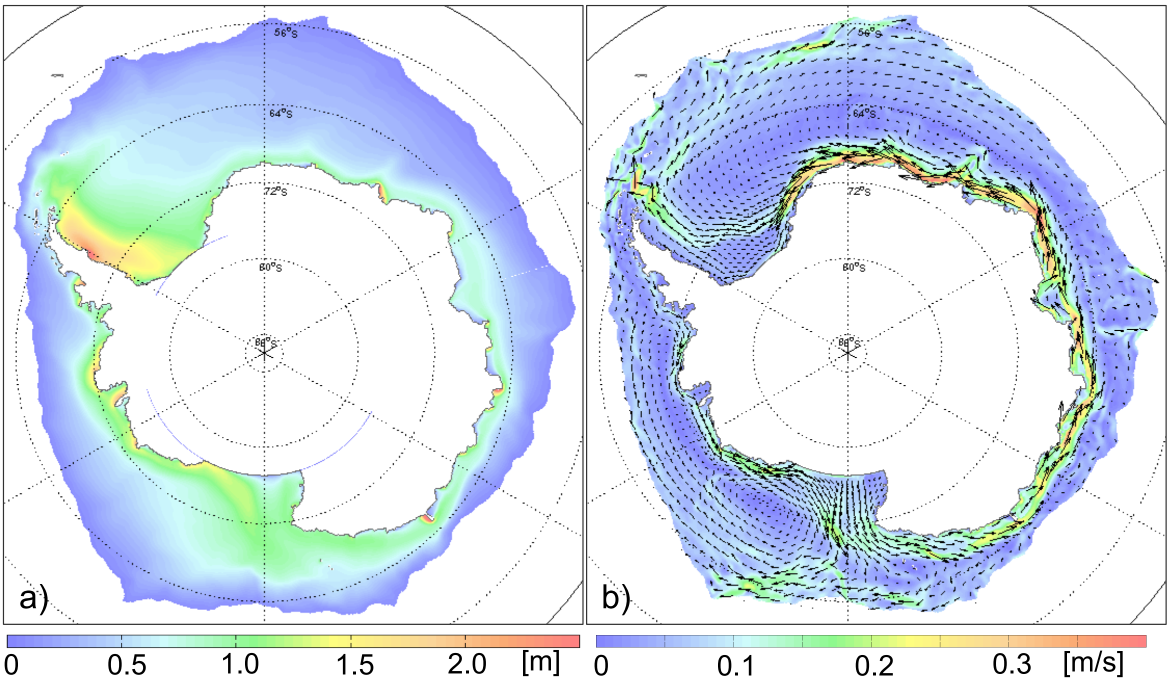

Figure S2: a) Mean sea ice thickness in CTR, April-September 2004-2013. b) Mean sea ice velocity in CTR, April-September 2004-2013.

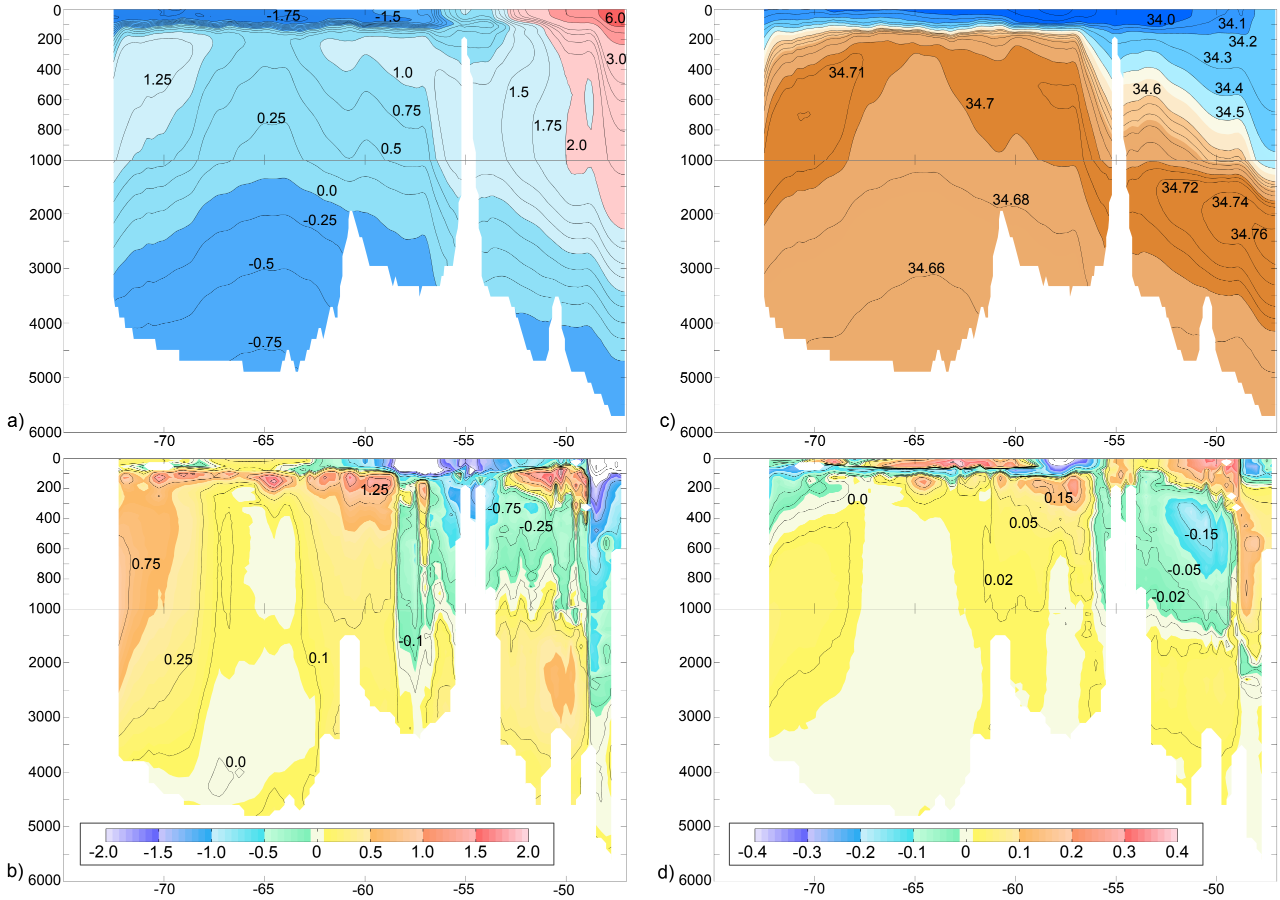

Figure S3: Section through the Weddell Sea (WOCE A23). a) CTR pot. temperature, b) difference to observed pot. temperature (Orsi and Whitworth, 2005), c) CTR salinity, d) difference to observed salinity (Orsi and Whitworth, 2005).

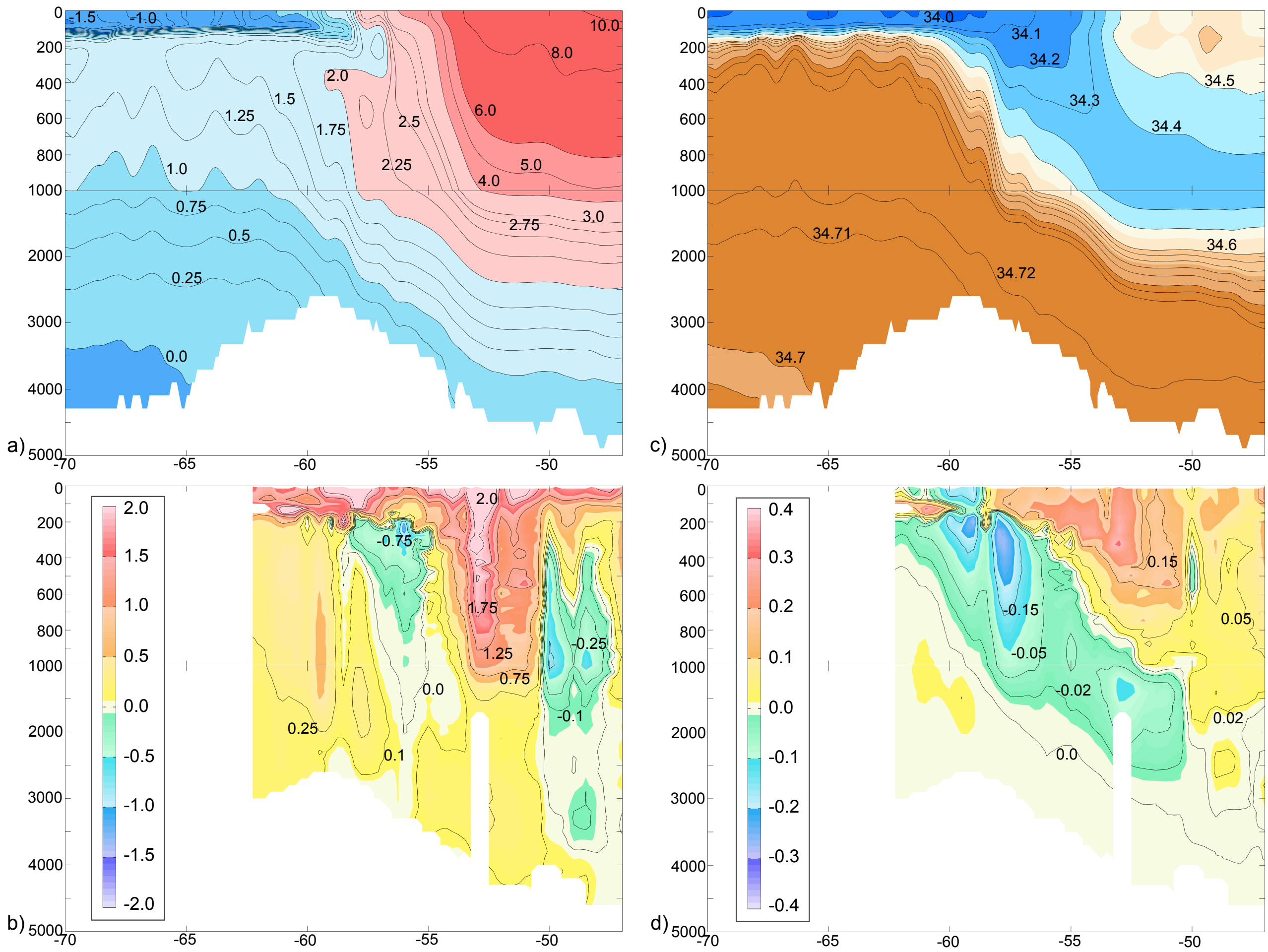

Figure S4: Section at 150° W (WOCE P16). a) CTR pot. temperature, b) difference to observed pot. temperature (Orsi and Whitworth, 2005), c) CTR salinity, d) difference to observed salinity (Orsi and Whitworth, 2005).